Electronic Supplementary Material (ESI) for Journal of Materials Chemistry A.

Supporting information

Structural stability enables high thermoelectric performance in room temperature Ag_2Se

Priyanka Jood*, Raju Chetty, Michihiro Ohta*

Global Zero Emission Research Center, National Institute of Advanced Industrial Science and Technology (AIST), Umezono 1-1-1, Tsukuba, Ibaraki 305-8568, Japan

p.jood@aist.go.jp

ohta.michihiro@aist.go.jp

Experimental Procedures

Sample preparation

Elemental silver (Ag; 99.999% pure; Kojundo Chemical Laboratory), selenium (Se; 99.9% pure; Kojundo Chemical Laboratory), and sulfur (S; 99.9999% pure; Kojundo Chemical Laboratory) were used as starting materials without further purification. Several ingots with nominal compositions given by Ag_2SeCh_y ($y = 0$, 0.005, 0.01, 0.015, 0.02, 0.04, 0.06 and 0.07; Ch = Se and S) and weighing 8 g each were synthesized by mixing appropriate amounts of Ag, Se, and S in carbon-coated fused silica tubes measuring 12 and 10 mm in outer and inner diameters, respectively. For example, 5.7852 g of Ag, 2.1173 g of Se, and 0.0086 g of S were mixed to prepare $Ag_2SeS_{0.01}$. Each silica tube was evacuated under a pressure of ~10^{-3} Pa and subsequently flame-sealed. All mixtures were heated to 1273 K at a rate of 65 K h^{-1} prior to being held at that temperature for 12 h, and subsequently cooled to 723 K at 11 K h^{-1}. The ingots were then annealed at 723 K for 24 h followed by cooling to room temperature in 15 h. Finally, the ingots were cut into pellets for thermoelectric-property measurement.

Crystal and defect structure analysis

Crystal structures of ingots were examined via X-ray diffractometry (XRD; MiniFlex; Rigaku) using Cu Kα radiations over a 2θ range of 20–60°. Prior to the examination, ingots were crushed and hand-ground to measure powder XRD patterns. Lattice parameters concerning powdered samples were refined using and integrated X-ray powder-diffraction software—Rigaku.

Microstructures and chemical compositions of ingots were examined using scanning electron microscopy (SEM; 15 kV; Miniscope TM 3030Plus; Hitachi high-Technologies) coupled with energy-dispersive X-ray spectroscopy (EDX; Quantax 70; Bruker). Transmission electron microscopy (TEM), energy-dispersive X-ray spectroscopy (EDX), electron diffraction (ED), and scanning transmission electron microscopy (STEM) investigations were performed at JEOL, Japan, using the JEM-ARM200F atomic resolution analytical electron microscope operated at 200 kV. To facilitate this investigation, samples were first polished via ion milling, and subsequently, grains with preferred orientations were selected using electron backscatter diffraction (EBSD). The selected grains were finally thinned using a focused ion beam (FIB).

Electrical transport measurements

Values of the Seebeck coefficient and electrical resistivity were measured simultaneously in a He atmosphere using the temperature differential and four-probe methods (ZEM-3; ULVAC-RIKO), respectively, over the 300–375-K temperature range. Typical dimensions of bars used for measurements equaled 2 × 2.5 × 8 mm. As observed, values of the Seebeck coefficient and electrical resistivity were reproducible over heating and cooling cycles for all samples, and relative uncertainties in determination of the Seebeck coefficient and electrical resistivity were estimated to be within 5%.

The Hall coefficient (R_H) was measured at room temperature using a home-built system under a magnetic field with strength of up to 2.3 T. Typical sample dimensions equaled 5 × 5 × 0.5 mm. Cu contact wires were attached to samples using an In-rich In–Ga paste.

Thermal transport measurements

Thermal conductivity (κ_{total}) values were calculated using the expression $\kappa_{\text{total}} = DC_{\text{p}}d$ involving thermal diffusivity (D), heat capacity (C_{P}), and density (d) of the material. The D values were directly measured, whereas C_{P} values were derived using a standard sample (Pyroceram 9606; Netzsch) using the laser flash method (LFA 457 MicroFlash; Netzsch) in an Ar gas flow (100 ml min^{-1}) over the 300–375-K temperature range. Discs with 10-mm diameter and 2-mm thickness were used as typical measurement samples. Sample surfaces were graphite coated to improve their emission and absorption properties. Additionally, C_{P} of two samples—Ag_2Se and $Ag_2Se_{1.01}$—were measured using Netzsch differential scanning calorimetry (DSC 404 F3 Pegasus) in an Ar atmosphere, and results obtained were similar to those obtained using LFA. Samples for DSC measurements were discs with 5-mm diameter and 1-mm thickness. As observed, values of D were reproduced over heating and cooling cycles for all samples. The D and C_{P} values are depicted in Figures. S1 and S2 in ESI. Density values for samples were determined using the gas pycnometer method (Accu Pyc II 1340; Micromeritics). All samples demonstrate densities ≥ 98% of their theoretical value (Table S1).

The relative uncertainty in thermal conductivity measurement was estimated to be within 6% when considering uncertainties in the determination of D, C_{P}, and d. The combined relative uncertainty in all measurements involved in ZT calculation equaled approximately 11%.

The sound velocities in the longitudinal and transverse modes were measured at room temperature using the pulse-echo method employing ultrasonic pulsers/receivers (5077PR; Olympus), 5- and 15-MHz longitudinal-contact transducers (V110-RM and V113-RM; Olympus), 5-MHz transverse-contact transducer (V156-RM; Olympus), and digitizing oscilloscope (WaveJet300A; Teledyne LeCroy).

Simulation of power generation characteristics

Three-dimensional finite-element simulations were performed using COMSOL Multiphysics equipped with a heat-transfer module to investigate power-generation characteristics of a single $Ag_2SeS_{0.01}$ thermoelectric element. A geometrical model with dimensions identical to the experimental element was used to calculate the electric power and heat-flow outputs. Fourth-order polynomial fittings of temperature-dependent S, σ, and κ_{total} values of the $Ag_2SeS_{0.01}$ element wer e used as material properties, and three-dimensional distributions of electric current density (J), heat flux (q), electrical potential (V), and temperature (T) were simulated using the said model. Values of the electric current I and output heat flow $Q_{out}(I)$ were calculated using J and q, respectively. The output power (P) reaches the maximum value when the electrical load is matched to the internal resistance of the thermoelectric element. The conversion efficiency (η) of the simulated thermoelectric element was calculated using the following relation.

$$\eta(I) = \frac{P(I)}{P(I) + Q_c(I)}$$

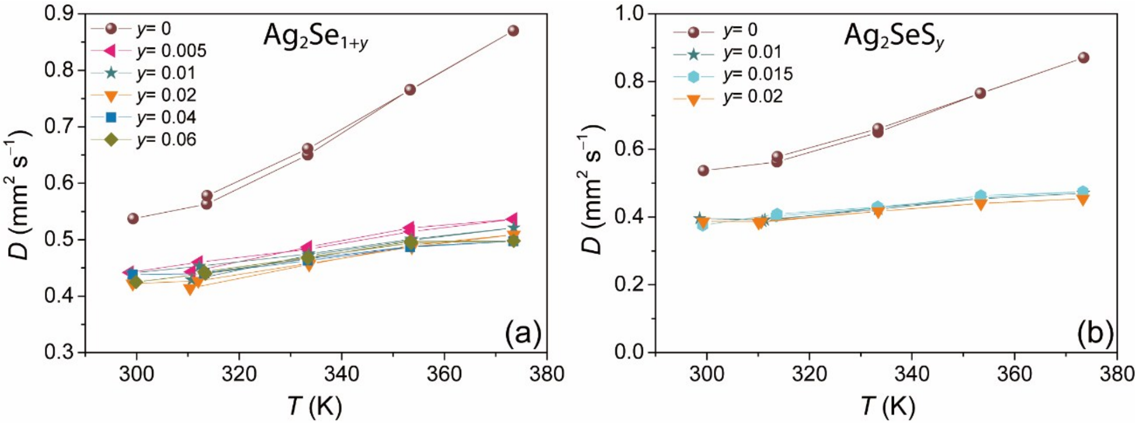

Figure S1 Temperature dependence of the thermal diffusivity (D) for (a) Ag_2Se_{1+y} (y = 0–0.06) and (b) Ag_2SeS_y (y = 0–0.02).

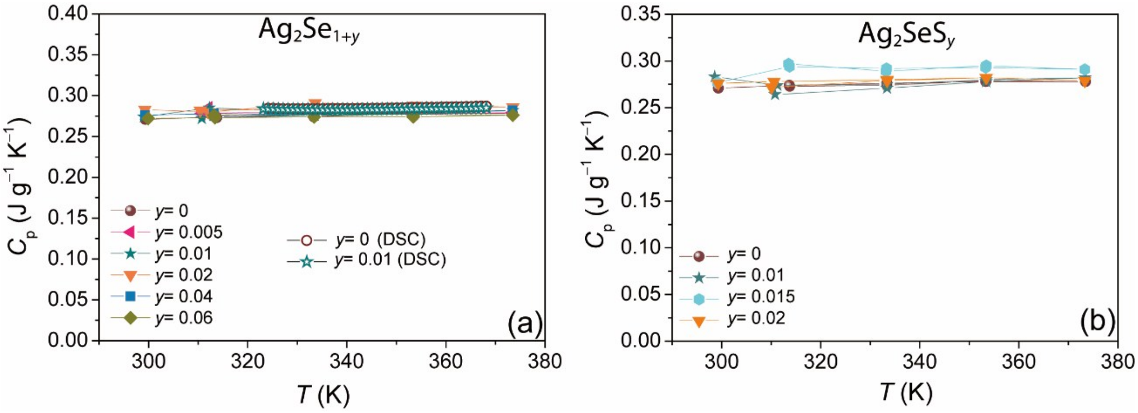

Figure S2 Temperature dependence of the heat capacity (Cp) for (a) Ag_2Se_{1+y} (y = 0–0.06) and (b) Ag_2SeS_y (y = 0–0.02) measured using laser flash method. Cp of Ag_2Se and $Ag_2Se_{1.01}$ measured using differential scanning calorimetry (DSC) is also presented.

Table S1 Density (*d*) and room temperature Hall coefficient (R_H) of Ag_2SeCh_y (y= 0 – 0.07, *Ch*= Se, S).

Sample	***d* (g cm^{-3})**	**R_H (10^{-6} m^3 C^{-1})**
Ag_2Se	8.17	–0.97
$Ag_2Se_{1.005}$	8.21	–1.65
$Ag_2Se_{1.01}$	8.23	–1.66
$Ag_2Se_{1.02}$	8.14	–1.66
$Ag_2Se_{1.04}$	8.00	–1.73
$Ag_2Se_{1.06}$	7.98	–1.70
$Ag_2SeS_{0.01}$	8.2	–1.70
$Ag_2SeS_{0.015}$	8.17	–1.71
$Ag_2SeS_{0.02}$	8.16	–1.66

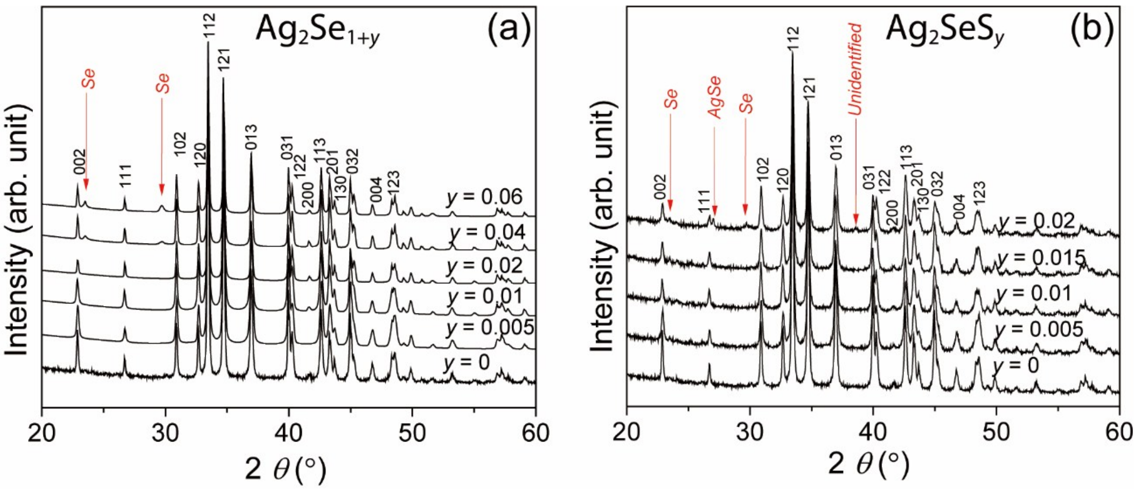

Figure S3 Powder X-ray diffraction patterns for (a) Ag_2Se_{1+y} (y = 0–0.06) and (b) Ag_2SeS_y (y = 0–0.02). Peaks for Se based impurities can be observed for $y \geq 0.02$.

The chemical state and coordination environment of Se contained in stoichiometric silver selenide (Ag_2Se) and minute anion excess sample ($Ag_2Se_{1.01}$) was analysed using Se K-edge X-ray absorption fine structure (XAFS) measurement which includes X-ray absorption near edge structure (XANES) spectra. The measurement was performed at Aichi Synchrotron Radiation Center (Aichi SR), Si (111) 2-crystal monochromator, and Se K-edge (12654.5 eV) absorption edge.

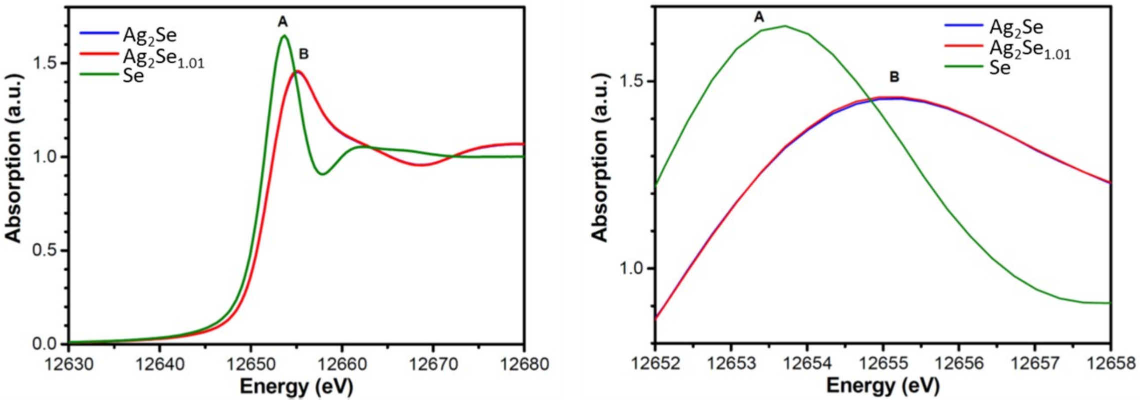

Figure S4 Se K-edge XANES spectra of Ag_2Se, $Ag_2Se_{1.01}$ and Se metal. XANES spectra depend on the chemical state or coordination structure of a designated element.

In the XANES spectrum of Se metal, main sharp peak **A** at 12654 eV was identified. Whereas, in the spectra of Ag_2Se and $Ag_2Se_{1.01}$, main broad peak **B** at 12655 eV was confirmed. These spectral differences are attributed to the difference in chemical state and/or atomic coordination environment of Se in silver selenide compound and Se metal.

$Ag_2Se_{1.01}$ has the same chemical state and coordination environment of Se as Ag_2Se due to the correspondence of the spectral shapes. However, the intensity of the main peak **B** of $Ag_2Se_{1.01}$ is slightly larger than that of Ag_2Se which could be due to minute Se richness in the former. No spectra related to Se metal is seen in $Ag_2Se_{1.01}$ which shows that no Se secondary phase exist in this sample.

Electron Backscatter Diffraction (EBSD) was performed on the Ag_2Se sample to characterize the observed triangular precipitates. EBSD analysis was carried out by the softwares, TSL OIM Data Collection 5.31 and TSL OIM Analysis 5.

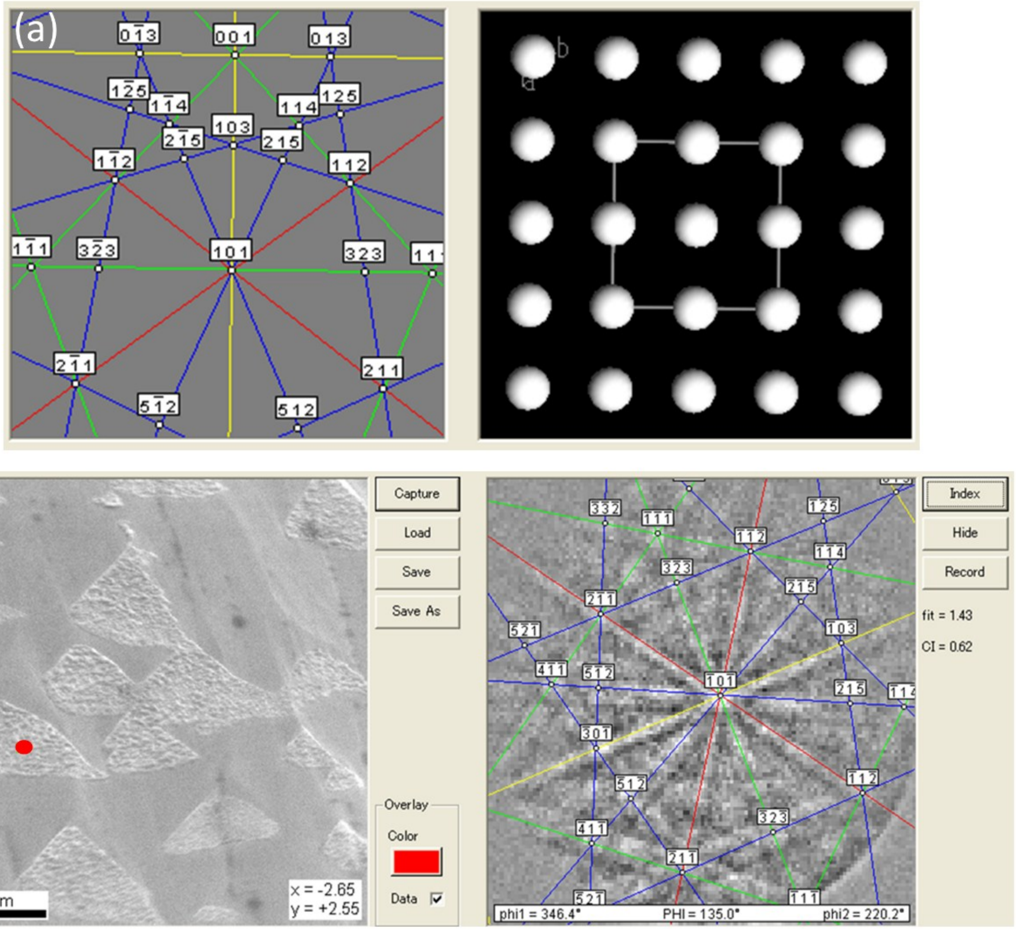

x = -2.65
y = +2.55

fit = 1.43
CI = 0.62

phi1 = 346.4°
PHI = 135.0°
phi2 = 220.2°

Figure S5 (a) Screen shots of TSL data file for Ag Cubic phase [m3m]. (b) screenshot showing the red dot (triangular precipitate) matching the database for Ag cubic phase.

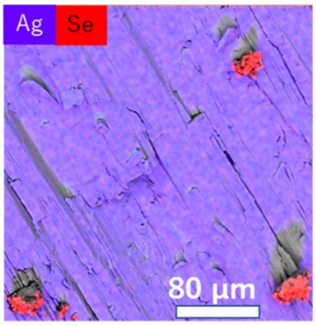

Figure S6 Scanning electron microscopy (SEM) and overlapping energy-dispersive X-ray spectroscopy (EDX) image of fractured area of $Ag_2Se_{1.02}$ showing Se precipitates.

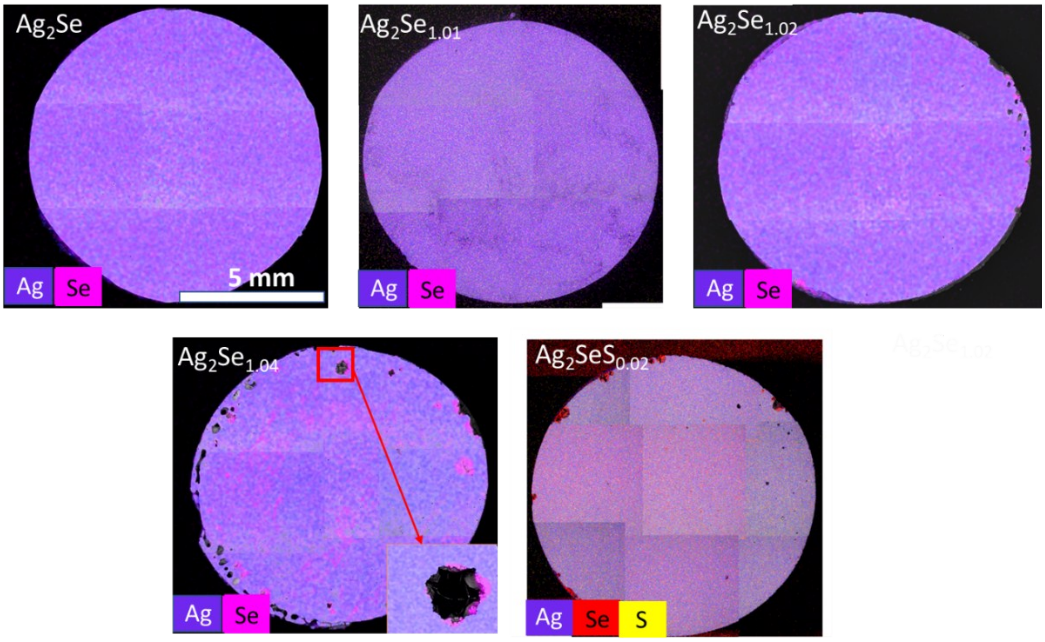

Figure S7 Scanning electron microscopy (SEM) and overlapping energy-dispersive X-ray spectroscopy (EDX) image of the diced surface of the ingot of selected samples (Ag_2SeCh_y ($y = 0 – 0.04$, Ch= Se, S) showing the precipitation of Se at the edges and the pores made as a consequence of Se escaping from the ingot for samples with large anion excess ($y \geq 0.02$). These images were made by joining together the SEM performed individually on different areas of the ingot's surface after dicing.

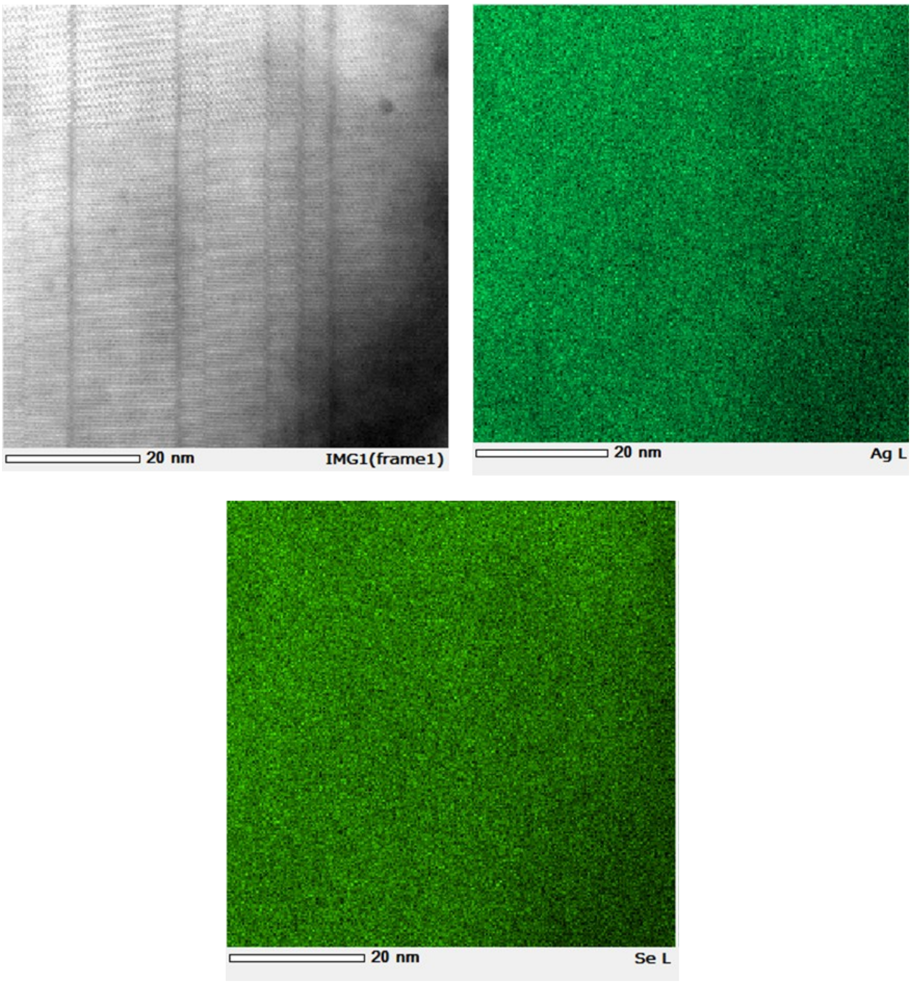

Figure S8 EDX scans of the region with metastable structures (dark contrasts) of Ag_2Se, showing slight Ag deficiency in the metastable structure.

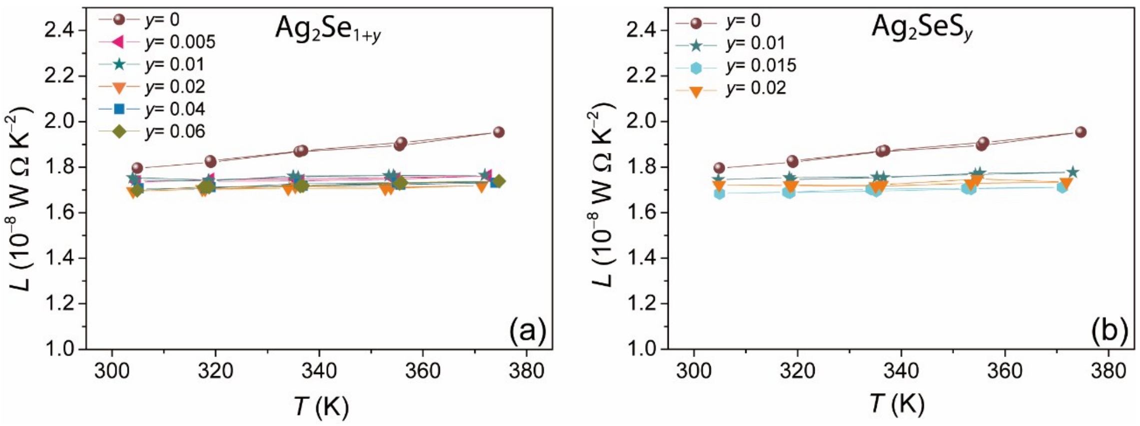

Figure S9 Temperature dependence of Lorenz number (*L*) for (a) Ag_2Se_{1+y} ($y = 0$–0.06) and (b) Ag_2SeS_y ($y = 0$–0.02). *L* was estimated using single parabolic band (SPB) model through the following equations.

The *L* can be expressed as a function of the reduced chemical potential (ζ^*) for a single parabolic band[1,2]:

$$L = \left(\frac{k_b}{e}\right)^2 \frac{3F_0(\zeta^*)F_2(\zeta^*) - 4F_1(\zeta^*)^2}{F_0(\zeta^*)^2} \qquad \text{(S1)}$$

ζ^* was obtained from the fitting of the experimental *S* values using the following equation for the single parabolic band model dominated by acoustic phonon scattering:

$$S = \frac{k_b}{e}\left(\frac{2F_1(\zeta^*)}{F_0(\zeta^*)} - \eta\right) \qquad \text{(S2)}$$

The Fermi integrals $F_m(\eta)$ are defined as:

$$F_m(\zeta^*) = \int_0^\infty \frac{x^m}{1 + exp(x - \zeta^*)} dx \qquad \text{(S3)}$$

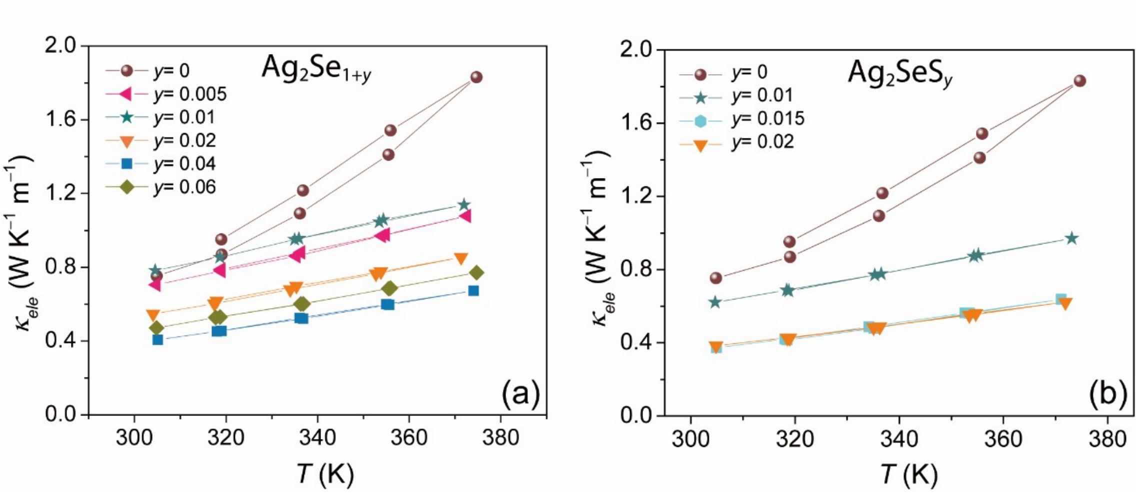

Figure S10 Temperature dependence of the electronic thermal conductivity (κ_{el}) for (a) Ag_2Se_{1+y} (y = 0–0.06) and (b) Ag_2SeS_y (y = 0–0.02). κ_{el} was calculated from: $\kappa_{\mathrm{el}} = LT\rho$ (L is the Lorenz number, and ρ is electrical resistivity).

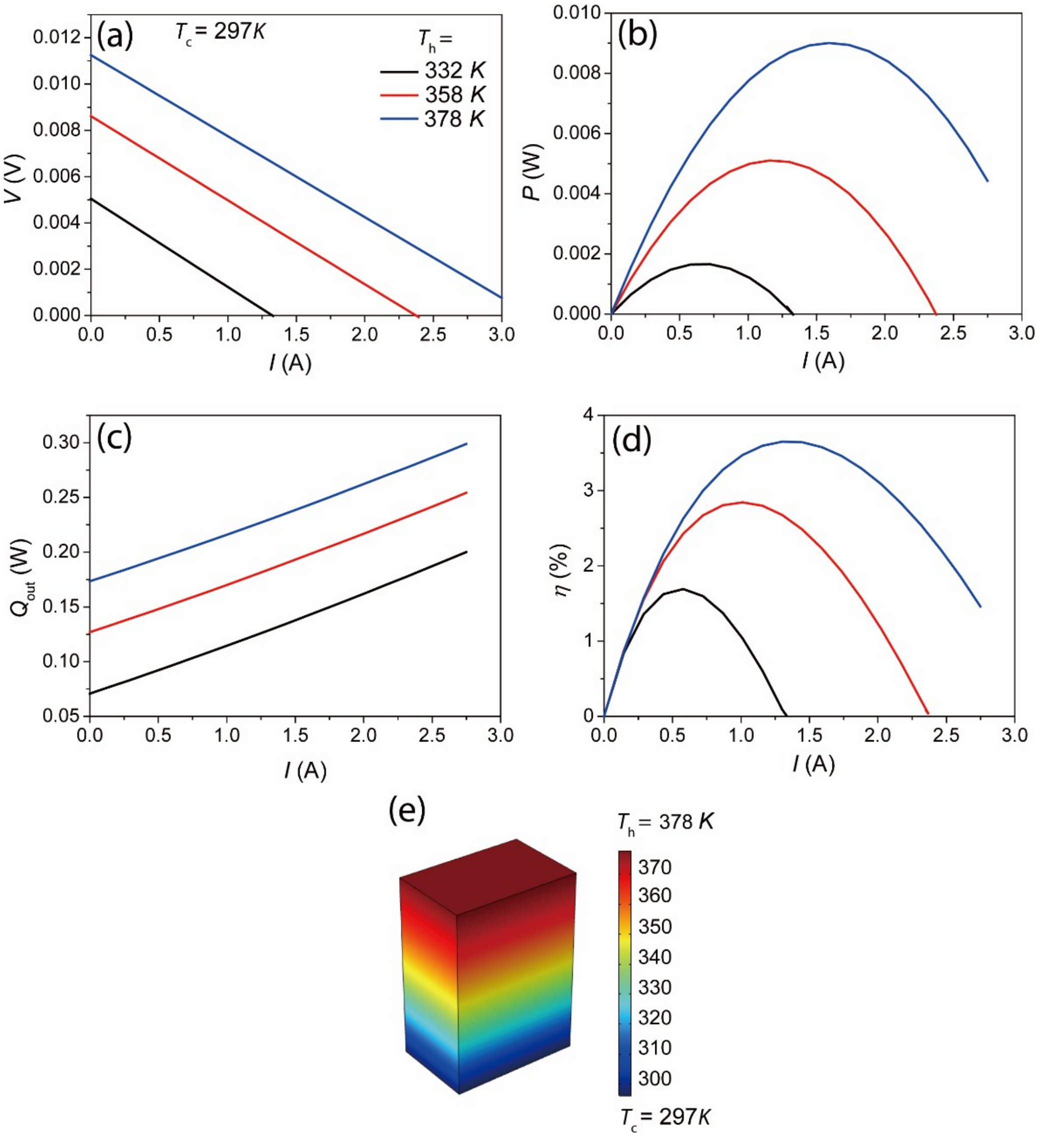

Figure S11 Based on the thermoelectric transport properties that were experimentally obtained in this study, the thermoelectric conversion parameters are simulated. (a) terminal voltage (V), (b) output power (P), (c) output heat flow (Q_{out}), and (d) conversion efficiency (η) of the $Ag_2SeS_{0.01}$ single thermoelectric element as a function of electrical current (I). (e) Simulated model of the $Ag_2SeS_{0.01}$ single thermoelectric element. The hot-side temperature (T_h) varied from 330 K to 380 K, whereas the cold-side (T_c) temperature was maintained at 297 K.

Electrical output power measurements

Electrical output power (P) of the $Ag_2SeS_{0.01}$ single thermoelectric element with Au electrodes and dimensions 3.089 mm × 4.683 mm × 6.673 mm, was measured under vacuum ($< 5 \times 10^{-2}$ Pa) by using a Mini-PEM (Advance Riko). The hot-side temperature (T_h) of thermoelectric element was varied from 330 K to 380 K, whereas the cold-side temperature (T_c) was maintained about 297 K.

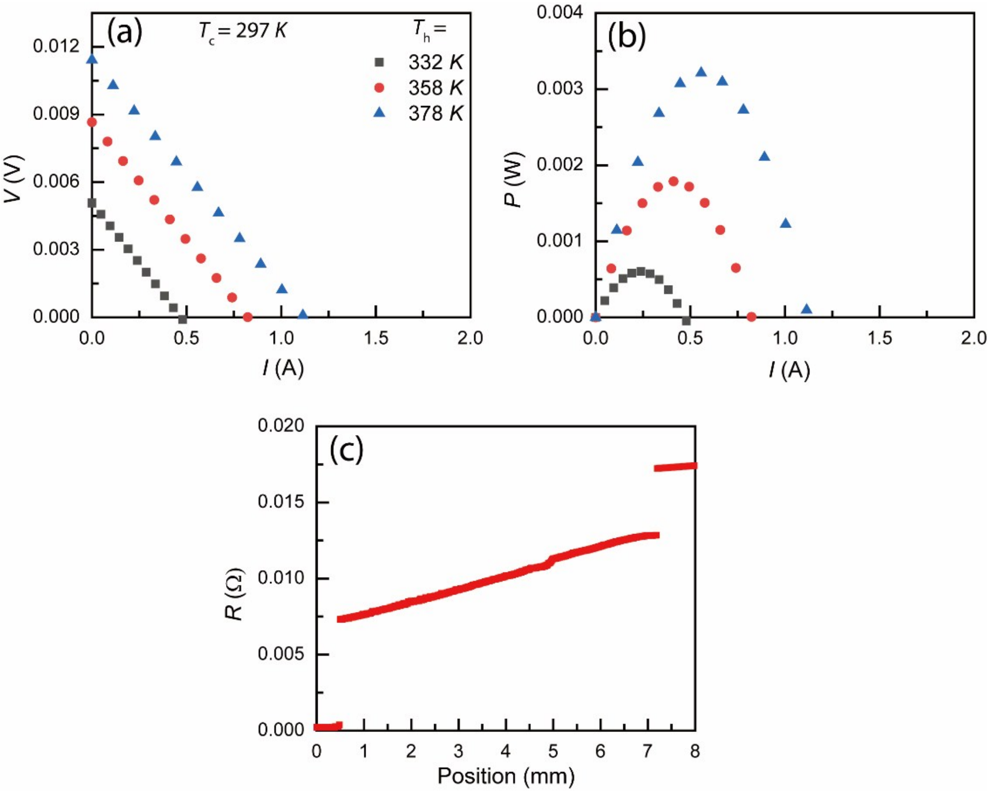

Figure S12 (a) Measured terminal voltage (V), electrical power output (P) of the $Ag_2SeS_{0.01}$ single thermoelectric element as a function of electrical current (I) (c) Electrical Contact between $Ag_2SeS_{0.01}$ and Au electrodes characterized by 4-probe mapping along the length at room temperature.

References

1. May, A.F., Fleurial, J.P., and Snyder, G.J. (2008). Thermoelectric performance of lanthanum telluride produced via mechanical alloying. *Phys. Rev. B - Condens. Matter Mater. Phys*. *78*, 1–12.
2. Johnsen, S., He, J., Androulakis, J., Dravid, V.P., Todorov, I., Chung, D.Y., and Kanatzidis, M.G. (2011). Nanostructures boost the thermoelectric performance of PbS. *J. Am. Chem. Soc*. *133*, 3460–3470.